J|A|C|S
ARTICLES
Published on Web 10/02/2002

Longitudinal ^{1}H Relaxation Optimization in TROSY NMR Spectroscopy

Konstantin Pervushin,* Beat Vögeli, and Alexander Eletsky

Contribution from the Laboratorium für Physikalische Chemie, Eidgenössische Technische Hochschule Hönggerberg, CH-8092 Zürich, Switzerland

Received June 3, 2002

Abstract: A general method to enhance the sensitivity of the multidimensional NMR experiments performed at high-polarizing magnetic field via the significant reduction of the longitudinal proton relaxation times is described. The method is based on the use of two vast pools of "thermal bath" ^{1}H spins residing on hydrogens covalently attached to carbon and oxygen atoms in ^{13}C,^{15}N labeled and fully protonated or fractionally deuterated proteins to uniformly enhance longitudinal relaxation of the $^1H^N$ spins and concomitantly the sensitivity of multipulse NMR experiments. The proposed longitudinal relaxation optimization is implemented in the 2D [^{15}N,^{1}H]-LTROSY, 2D [^{15}N,^{1}H]-LHSQC and 3D LTROSY-HNCA experiments yielding the factor 2−2.5 increase of the maximal signal-to-noise ratio per unit time at 600 MHz. At 900 MHz, the predicted decrease of the $^1H^N$ longitudinal relaxation times can be as large as one order of magnitude, making the proposed method an important tool for protein NMR at high magnetic fields.

Introduction

The application of nuclear magnetic resonance (NMR) spectroscopy to structure determination of proteins and nucleic acids[1] with molecular masses exceeding 30 kDa is largely constrained by two factors, the fast transverse relaxation of spins of interest and the complexity of NMR spectra, both of which increase with increasing molecular size.[2−5] The TROSY technique offers a simple and robust bypass solution to both of these problems when NMR spectroscopy is conducted at sufficiently high magnetic fields.[6] What is less appreciated as a factor limiting the sensitivity is the long longitudinal relaxation of the ^{1}H spins at high magnetic fields and larger molecular weights.[1] Long longitudinal relaxation times, which for proteins with MWs above 30 kDa are typically found to be in the range of many seconds,[7] result in a substantial loss of the signal-to-noise of the multipulse NMR experiments per unit time of the data acquisition.[8] Thus, any enhancement of longitudinal relaxation increases the sensitivity of NMR experiments.

Thus far, methods used to enhance longitudinal relaxation include the use of paramagnetic compounds such as MRI contrasting reagents,[9,10] naturally occurring paramagnetic metal centers,[11−13] fast exchange of the labile protons with water in the SEA-TROSY experiment.[14,15] The limitations of these methods stem from their abilities to enhance sensitivity only of the very limited subset of the ^{1}H spins. For the special HMQC class of heteronuclear correlation experiments, implementation of the Ernst angle[8] might yield signal enhancement on the order of 25% by accounting for the finite rate of recovery to the thermal equilibrium.[16] A sensitivity gain in the range of 10−20% in TROSY spectroscopy can be obtained by an alternative approach that utilizes the intermediate storage of a part of the steady-state magnetization of spin I on insensitive spin S with a pulse sequence element ISIS during the interscan delay.[17] Although the later represents a general spectroscopic technique, the achieved gain is rather modest.

Here, we propose the use of two vast pools of ^{1}H spins residing on hydrogens covalently attached to carbon and oxygen atoms in ^{13}C, ^{15}N, or ^{15}N labeled and fully protonated or fractionally deuterated proteins to significantly and uniformly enhance longitudinal relaxation of the $^1H^N$ spins and concomitantly the sensitivity of multipulse NMR experiments. The NMR experiments with the excitation/detection performed with the $^1H^N$ spins covalently attached to the ^{15}N spins are designed for the assignment of the backbone resonances and collect ion

* To whom correspondence should be addressed. Phone: +41-1-6320922. Fax: +41-1-6321021. E-mail: kopeko@phys.chem.ethz.ch.

(1) Wuthrich, K. *NMR of Proteins and Nucleic Acids*; Wiley: New York, 1986.
(2) Wagner, G. *J. Biomol. NMR* **1993**, *3*, 375−385.
(3) Kay, L. E.; Gardner, K. H. *Curr. Opin. Struct. Biol.* **1997**, *7*, 722−731.
(4) Clore, G. M.; Gronenborn, A. M. *Nat. Struct. Biol.* **1997**, *4 Suppl*, 849−853.
(5) Clore, G. M.; Gronenborn, A. M. *Curr. Opin. Chem. Biol.* **1998**, *2*, 564−70.
(6) Pervushin, K.; Riek, R.; Wider, G.; Wuthrich, K. *Proc. Natl. Acad. Sci. U.S.A.* **1997**, *94*, 12 366−12 371.
(7) Wang, Y. X.; Jacob, J.; Cordier, F.; Wingfield, P.; Stahl, S. J.; Lee-Huang, S.; Torchia, D.; Grzesiek, S.; Bax, A. *J. Biomol. NMR* **1999**, *14*, 181−184.
(8) Ernst, R. R.; Bodenhausen, G.; Wokaun, A. *The Principles of Nuclear Magnetic Resonance in One and Two Dimensions*; Oxford: Clarendon, 1987.
(9) Pintacuda, G.; Otting, G. *J. Am. Chem. Soc.* **2002**, *124*, 372−373.
(10) Liepinsh, E.; Baryshev, M.; Sharipo, A.; Ingelman-Sundberg, M.; Otting, G.; Mkrtchian, S. *Structure* **2001**, *9*, 457−471.
(11) Machonkin, T. E.; Westler, W. M.; Markley, J. L. *J. Am. Chem. Soc.* **2002**, *124*, 3204−3205.
(12) Chen, Z. G.; Deropp, J. S.; Hernandez, G.; Lamar, G. N. *J. Am. Chem. Soc.* **1994**, *116*, 8772−8783.
(13) Krugh, T. R.; Schaefer, W. C. *J. Magn. Reson.* **1975**, *19*, 99−107.
(14) Pellecchia, M.; Meininger, D.; Shen, A. L.; Jack, R.; Kasper, C. B.; Sem, D. S. *J. Am. Chem. Soc.* **2001**, *123*, 4633−4634.
(15) Pellecchia, M.; Meininger, D.; Dong, Q.; Chang, E.; Jack, R.; Sem, D. S. *J. Biomol. NMR* **2002**, *22*, 165−173.
(16) Ross, A.; Salzmann, M.; Senn, H. *J. Biomol. NMR* **1997**, *10*, 389−396.
(17) Riek, R. *J. Biomol. NMR* **2001**, *21*, 99−105.

10.1021/ja027149q CCC: $22.00

structural constraints with larger proteins at high magnetic fields and frequently utilize the TROSY principle.[6] The proposed longitudinal relaxation optimization is implemented in the 2D [^{15}N,^{1}H]-LTROSY, 2D [^{15}N,^{1}H]-LHSQC, and 3D LTROSY−HNCA experiments yielding the factor 2−2.5 increase of the maximal signal-to-noise per unit time measured with two proteins, 7 kDa ubiquitin (PDB code 1UBI) and 44 kDa trimeric *B. Subtilis* chorismate mutase (PDB code 1COM). Calculations predict that the optimal interscan d_1 delays in the longitudinal relaxation optimized NMR experiments can be an order of magnitude shorter than those in the conventional experiments. Thus, the longitudinal relaxation optimization might become an important tool for NMR of proteins at 900 MHz.

Methods

Signal-to-Noise per Unit Time and Longitudinal ^{1}H Relaxation. The repetition rate of an NMR experiment is a function of the interscan delay d_1 performed between the last pulse of one scan to the first pulse of the next scan. The signal-to-noise ratio per measurement time, referred as the sensitivity of the experiment, is given by eq 1[8]

$$S/N_t = c(1 - \exp(-Rd_1))/\sqrt{d_0 + d_1} \quad (1)$$

where the R is the longitudinal relaxation rate of the excited spins, d_0 is the duration of the pulse sequence excluding data acquisition, d_1 is the interscan delay, and c is a proportionality coefficient. For monoexponential relaxation, the maximal sensitivity $S/N_{tmax} = c0.71/\sqrt{d^{opt}}_1 \sim c0.64\sqrt{R}$ is achieved at the optimal interscan delay $d_1{}^{opt} = 1.25/R - d_0$. Thus, the efficiency of longitudinal relaxation of the excited spins defines the sensitivity of NMR experiments in the case, where many repetitions of the excitation/detection cycles are performed.

Longitudinal relaxation of the ^{1}H spins, I_z, to the thermal equilibrium, I_z^{eq}, can be modeled by the system of linear differential equations given by eq 2, which are inhomogeneous with respect to exchangeable protons in OH, NH_3^+, COOH, guanidinium groups, and structural water molecules[18]

$$dI_z/dt = \mathbf{R}(I_z - I_z^{eq}) + \mathbf{K}I_z \quad (2)$$

where $\mathbf{R}$ is the relaxation matrix,[8] $\mathbf{K}$ is the kinetic matrix collecting chemical exchange constants between the individual ^{1}H spins and water,[1,19] I_z is a column vector consisting of the four groups of spins, I_z^N, I_z^C, I_z^O, and I_z^W, which represent the ^{1}H spins covalently attached to the ^{15}N, ^{13}C, and ^{16}O atoms, and residing on the water molecules, respectively. During the numerical integration of eq 2, the boundary condition $I_z^W(t) - I_z^W(0) = 0$ is maintained assuming that (i) the longitudinal relaxation time of water protons is significantly longer than that of the protein ^{1}H spins and (ii) the protein solution is sufficiently diluted. The initial values of the I_z^N, I_z^C, I_z^O, and I_z^W spins are set according to the condition of the corresponding magnetization after signal acquisition in analyzed NMR experiments. For each individual amide proton, d_1^{opt} is reported as a time point, at which the global maximum of the function $I_z^N(t)/\sqrt{t}$ occurs for $t > 0$, thus avoiding the problem of the deconvolution of the multiple exponential time course of the function $I_z^N(t)$.

Longitudinal Relaxation Optimized NMR Experiments. TROSY-type heteronuclear correlation experiments[6,20−26] select the two coherence transfer pathways obtained in alternate scans connecting the single transition of the heteronuclear N spin with the single transition of spin I

$$I_z^N \rightarrow N_{12}{}^+ \rightarrow I^N{}_{13}{}^- \quad (3.1)$$

$$I_z^N \rightarrow N_{12}{}^- \rightarrow I^N{}_{13}{}^- \quad (3.2)$$

The single-transition basis operators refer to the transitions 1→2 and 3→4 of spin N and 1→3 and 2→4 of spin I in the standard energy-level diagram for a system of two spins 1/2. The sensitivity of these experiments is not compromised when a heteronuclear gradient echo is applied[20,27] providing efficient elimination of the water resonance from the resulting spectrum.

In addition to the magnetization transfer pathways given by eqs 3, the experimental scheme of Figure 1a controls two additional magnetization flows given by eqs 4 and 5 outlining the evolution of the density operators of the I_z^C and I_z^W spin groups, respectively

$$I_z^C \rightarrow C_zI_z^C \rightarrow \pm I_z^C \quad (4)$$

$$I_z^W \rightarrow I_x^W \rightarrow \pm I_z^W \quad (5)$$

where the "plus" or "minus" signs can be arbitrarily controlled. For example, the "minus" sign in eq 4 can be selected by removing the ^{13}C 180° pulse ψ_1 from the experimental scheme of Figure 1a otherwise the "plus" sign is obtained. The longitudinal ^{1}H relaxation optimization occurs when both positive signs for the magnetization transfer pathways of eqs 4 and 5 are selected.

Similar considerations allow the control of the parallel magnetization transfer pathways in the experimental schemes of Figure 1b,c. In these cases, the separation between I^N and I^C transfer pathways is achieved by applying $^1H^N$ band selective 90° excitation pulses using the distinct difference between chemical shifts of the amide and aliphatic protons. In the case of the 3D LTROSY-HNCA experiment the TROSY-type transverse relaxation optimization is employed during the long N→C and C→N polarization transfer periods.

Results and Discussion

To enhance longitudinal $^1H^N$ relaxation in the experimental schemes of Figure 1 three independent magnetization transfer pathways are constructed. The main pathway transfers the steady-state $^1H^N$ magnetization to the directly attached ^{15}N spin and back for the signal acquisition. This pathway defines the type of the NMR experiment performed. In the case of TROSY of Figure 1a, the main pathway is outlined by eqs 3.[20] The $^1H^C$ pathway represented by eq 4 returns the steady-state $^1H^C$ magnetization to the z direction after the last 90° ^{1}H pulse of the pulse sequence. During the t_1 chemical shift evolution period, the $^1H^C$ magnetization is stored as a slowly relaxing two spin order operator $C_zI_z^C$.[28] The steady state of the $^1H^C$ magnetization can be controlled by executing or omitting the 180° ^{13}C pulse ψ_1 in Figure 1a. The inversion of the I_z^C at the beginning of the signal acquisition results in the rapid saturation of the $^1H^C$ magnetization and as a consequence retarded return of the $^1H^N$ spins to the steady-state. The evolution pathway of water magnetization is represented by eq 5. During the t_1

(18) Otting, G.; Liepinsh, E.; Wuthrich, K. *Science* **1991**, *254*, 974−980.
(19) Englander, S. W.; Mayne, L.; Bai, Y.; Sosnick, T. R. *Protein Sci.* **1997**, *6*, 1101−1109.
(20) Pervushin, K.; Wider, G.; Wuthrich, K. *J. Biomol. NMR* **1998**, *12*, 345−348.
(21) Czisch, M.; Boelens, R. *J. Magn. Reson.* **1998**, *134*, 158−160.
(22) Weigelt, J. *J. Am. Chem. Soc.* **1998**, *120*, 10 778−10 779.
(23) Brutscher, B.; Boisbouvier, J.; Pardi, A.; Marion, D.; Simorre, J. P. *J. Am. Chem. Soc.* **1998**, *120*, 11 845−11 851.
(24) Andersson, P.; Annila, A.; Otting, G. *J. Magn. Reson.* **1998**, *133*, 364−367.
(25) Meissner, A.; Schulte-Herbruggen, T.; Briand, J.; Sorensen, O. W. *Mol. Phys.* **1998**, *95*, 1137−1142.
(26) Rance, M.; Loria, J. P.; Palmer, A. G. *J. Magn. Reson.* **1999**, *136*, 92−101.
(27) Kay, L. E.; Keifer, P.; Saarinen, T. *J. Am. Chem. Soc.* **1992**, *114*, 10 663−10 665.

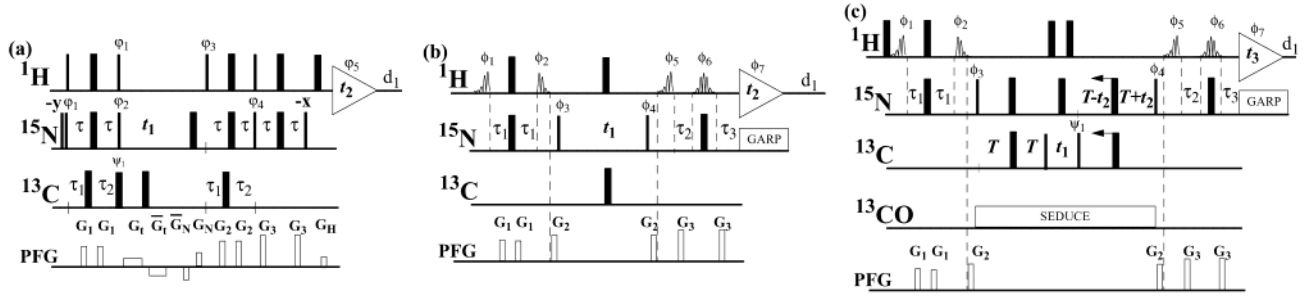

Figure 1. Experimental schemes for the longitudinal ^{1}H relaxation optimized (a) 2D [^{15}N,^{1}H]-LTROSY, (b) 2D [^{15}N,^{1}H]-LHSQC, and (c) 3D [^{15}N,^{1}H]-LTROSY-HNCA experiments. The radio frequency pulses on ^{1}H, ^{15}N, ^{13}C, ^{13}CO, and ^{1}H$^\alpha$ are applied at 4.7, 118, 55, 174, and 4.7 ppm, respectively. Narrow and wide black bars indicate nonselective 90° and 180° pulses, respectively. Complex shapes on the line marked ^{1}H indicate the ^{1}H^N band-selective 1.5 ms excitation E-Burp2 pulses[31] with the phases ϕ_1 and ϕ_5 and $\gamma B_1 = 2733$ Hz, the identical to the pulses ϕ_1 and ϕ_5 but time-reversed excitation E-Burp2 pulse with the phase ϕ_2 and the 1.8 ms refocusing Re−Burp pulse[31] with the phase ϕ_6 and $\gamma B_1 = 3050$ Hz. The center of the excitation of all ^{1}H^N band-selective pulses is placed at 9.7 ppm. The line marked PFG indicates the duration and strength of pulsed magnetic field gradients applied along the *z*-axis. The variable interscan ^{1}H relaxation delay d_1 is performed between repeated applications of the experimental pulse sequences. In (a), the delays are $\tau = 2.7$ ms, $\tau_1 = 1.7$ ms, and $\tau_2 = 2.0$ ms. The PFGs are G_1: 800 μs, 50 G/cm; G_2: 800 μs, 60 G/cm; G_3: 800 μs, 80 G/cm; G_t: $t_{1/2}$, 10 G/cm; $\bar{G}_t$: $t_{1/2}$, −10 G/cm; G_N: 800 μs, 50 G/cm; $\bar{G}_N$: 800 μs, −50 G/cm; G_H: 800 μs, 10.13 G/cm. The phases are $\varphi_1 = \{y\}$; $\varphi_2 = \{y, -y, x, -x\}$; $\varphi_3 = \{y\}$; $\varphi_4 = \{-y\}$; $\varphi_5 = \{y, -y, -x, x\}$; $\psi_1 = \{x\}$; $\{x\}$ for all other pulses. A phase-sensitive spectrum in the ^{15}N(t_1) dimension is obtained by recording a second FID for each t_1 value, with $\varphi_1 = \{-y\}$; $\varphi_2 = \{y, -y, -x, x\}$; $\varphi_3 = \{-y\}$; $\varphi_4 = \{y\}$; $\varphi_5 = \{-y, y, x, -x\}$, G_N: 800 μs, −50 G/cm; $\bar{G}_N$: 800 μs, 50 G/cm and data processing as described by[27]. The broad band inversion of the ^{13}C spins is achieved with the $90^o_x-225^o_y-90^o_x$ composite pulses.[28] To eliminate the effect of the longitudinal ^{1}H relaxation optimization, the ^{13}C composite pulse ψ_1 is not performed. In (b), the delays are $\tau_1 = 2.4$ ms, $\tau_2 = 2.34$ ms and $\tau_3 = 2.4$ ms. The PFGs are G_1: 800 μs, 50 G/cm; G_2: 800 μs, 70 G/cm; G_3: 800 μs, 80 G/cm. The phases are $\phi_1 = \{x\}$; $\phi_2 = \{y\}$; $\phi_3 = \{x,-x\}$; $\phi_4 = \{x,x,-x,-x\}$; $\phi_5 = \{x\}$; $\phi_6 = \{x\}$; $\phi_7 = \{x,-x,-x,x\}$; $\{x\}$ for all other pulses. Quadrature detection in the ^{1}H(t_2) dimension is achieved by the States-TPPI method[37] applied to the phase ϕ_3. To eliminate the effect of the longitudinal ^{1}H relaxation optimization 2ms ^{1}H spin lock pulse at a field strength of $\gamma B_1 = 20$ kHz employed to dephase the ^{1}H magnetization immediately after data acquisition. In (c), the delays are $\tau_1 = 2.4$ ms, $\tau_2 = 2.34$ ms, $\tau_3 = 2.4$ ms, and $T = 15$ ms. The PFGs are G_1: 800 μs, 50 G/cm; G_2: 800 μs, 70 G/cm; G_3: 800 μs, 80 G/cm. The phases are $\phi_1 = \{x\}$; $\phi_2 = \{y\}$; $\phi_3 = \{x,-x\}$; $\phi_4 = \{x,x,-x,-x\}$; $\phi_5 = \{x\}$; $\phi_6 = \{x\}$; $\phi_7 = \{x,-x,-x,x,-x,x,x,-x\}$; $\psi_1 = \{x,-x\}$; $\{x\}$ for all other pulses. Quadrature detection in the ^{13}C$^\alpha$(t_1) and ^{1}H(t_2) dimensions is achieved by the States-TPPI method[37] applied to the phases ψ_1 and ϕ_3, respectively. The ^{13}CO spins are decoupled by the SEDUCE composite pulse decoupling.[28] For the fractionally deuterated proteins, the experiment can be performed with ^{2}H-decoupling during t_1 achieved with WALTZ-16[38] at a field strength of $\gamma B_1 = 0.7$ kHz. In (b) and (c) ^{15}N spins are decoupled with GARP[28] at a field strength of $\gamma B_1 = 2.5$ kHz.

chemical shift evolution period transverse water magnetization is dephased and rephased by a pair of weak PFG pulses to prevent radiation damping. In the experimental scheme of Figure 1a, almost 90% of the initial water magnetization is recovered. Due to the fast chemical exchange between ^{1}H of water and majority of the O-bound ^{1}H spins the I_z^O magnetization quickly equilibrates with the I_z^W magnetization with k_{ex} of the order of 10^3 s^{-1}.[1]

As an application, the [^{15}N,^{1}H]-correlation spectrum of the 44 kDa trimeric *B. Subtilis* chorismate mutase (BsCM, PDB code 1COM) (Figure 2) was recorded with the LTROSY experiment of Figure 1a with (Figure 2a) and without (Figure 2b) the longitudinal relaxation optimization of the ^{1}H^N spins. In all of the spectra of Figure 2 water magnetization was flipped to the +z direction before signal acquisition. The protein was uniformly ^{15}N,^{13}C-labeled and 35% randomly deuterated, dissolved in 95% H_2O/5% D_2O at a concentration of 2 mM and pH = 7.5.[29] As expected, a uniform and significant improvement of sensitivity was observed. Figure 2c shows the spectrum measured with the conventional 2D [^{15}N,^{1}H]-TROSY[20] where water-flip-back pulses[30] were replaced with ^{1}H^C band-selective 1 ms E-Burp2 pulses[31] centered at 1.4 ppm with all ^{1}H spins resonating between 4.9 ppm and −2 ppm (including water) flipped to the +z direction before data acquisition. In that case, a substantial improvement of sensitivity is also observed (Figure 2c).

Systematic measurements of S/N_t as a function of the interscan delay d_1 were performed using the experimental schemes of

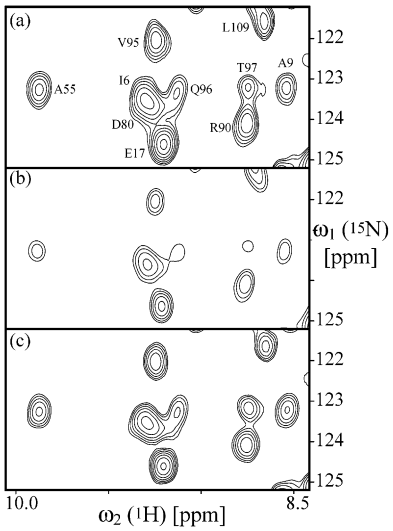

Figure 2. Region of the 2D [^{15}N,^{1}H]-LTROSY spectra of the u-[^{13}C,^{15}N]-labeled 44 kDa BsCM measured with the experimental scheme of Figure 1a, (a), with the ^{13}C 180° ψ_1 pulse applied and, (b), the ^{13}C 180° pulse ψ_1 is not performed. (c), The same spectrum measured with the conventional 2D [^{15}N,^{1}H]-TROSY[20] where the water selective pulses were replaced with ^{1}H^C band-selective 1 ms E-Burp2 pulses[31] with $\gamma B_1 = 4100$ Hz centered at 1.4 ppm. In (c), all ^{1}H spins resonating between 4.9 ppm and −2 ppm (including water) are flipped to the +z direction before data acquisition. For all spectra 140(t_1)*1024(t_2) complex points were accumulated yielding $t_{1max} = 20$ ms and $t_{2max} = 51.2$ ms, respectively, with the interscan ^{1}H relaxation delay $d_1 = 340$ ms and 4 scans per increment. The sequence specific resonance assignments of the cross-peaks are shown.

Figure 1, parts a and b, with two proteins, 7 kDa uniformly ^{15}N,^{13}C-labeled and uniformly ^{2}H,^{15}N,^{13}C-labeled ubiquitin and 44 kDa uniformly ^{15}N,^{13}C-labeled and 35% randomly deuterated and uniformly ^{2}H,^{15}N,^{13}C-labeled BsCM. Figure 3 shows a

(28) Cavanagh, J.; Fairbrother, W. J.; Palmer, A. G.; Skelton, N. J. *Protein NMR Spectroscopy: Principles and Practice*; Academic Press: New York, 1996.
(29) Eletsky, A.; Kienhöfer, A.; Pervushin, K. *J. Biomol. NMR* **2001**.
(30) Grzesiek, S.; Bax, A. *J. Am. Chem. Soc.* **1993**, *115*, 12 593−12 594.
(31) Geen, H.; Freeman, R. *J. Magn. Reson.* **1991**, *93*, 93−141.

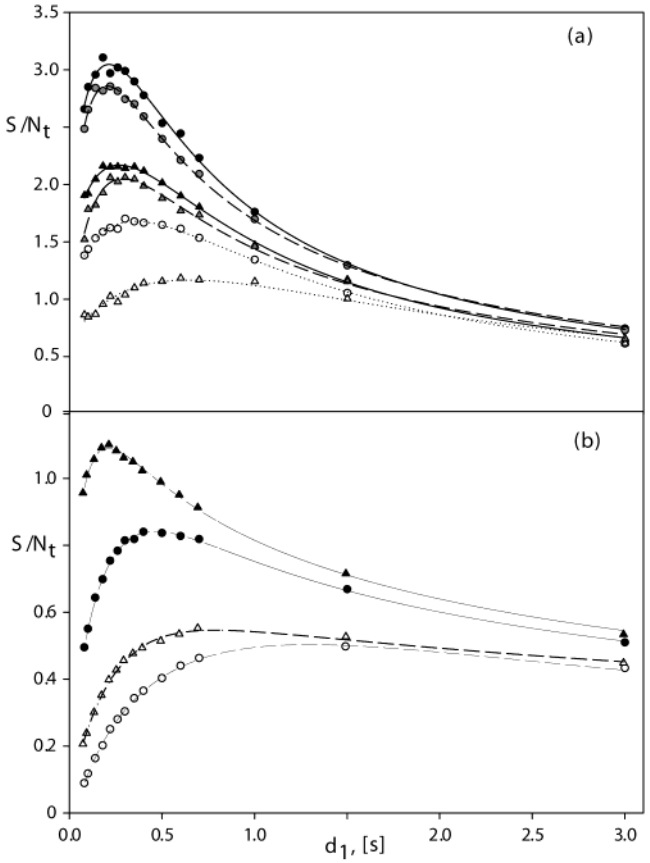

Figure 3. Signal-to-noise ratios per unit time, S/N_t, in a series of the 2D [^{15}N,^{1}H]-correlation spectra versus the interscan ^{1}H relaxation delay d_1 measured with (a) the u-[^{13}C,^{15}N]-labeled 7 kDa Ubiquitin and (b) the u-[^{13}C,^{15}N]-labeled 44 kDa BsCM. In (a) circles and triangles represent S/N_t measured for Gln2 and Ile13, respectively. The filled and open symbols indicate S/N_t obtained using the experimental scheme of Figure 1a with and without the ^{13}C 180° pulse ψ_1, respectively. The gray symbols represent S/N_t in a series of the 2D [^{15}N,^{1}H]-TROSY[20] experiments with the $^1H^C$ flip-back (see Caption to Figure 2c). In (b) circles and triangles represent S/N_t measured for Ala55 and Glu17, respectively. The open and filled symbols indicate S/N_t obtained using the experimental scheme of Figure 1b performed with and without 2ms ^{1}H spin lock pulse, respectively. The fit of the experimental relaxation rates using eq 1 are shown by solid and dashed lines.

2−2.5 times improvement of the maximal S/N_t achieved for both proteins in the protonated and fractionally deuterated states. An excellent fit between eq 1 and the experimental data is observed for both proteins (Figure 3). For the spectra measured with the longitudinal relaxation optimization the optimal d_1 delays corresponding to the maximal values of the S/N_t function are reduced by a factor of 4 on average as it is predicted from eq 1 and distributed in much narrower range than the optimal d_1 delays measured without optimization (Figure 4). On the other hand, no improvement in S/N_t was observed in the case where all nonexchangeable protons were replaced with deuterons (Figure 1 in the Supporting Information) establishing that the sensitivity enhancement mainly results from the construction of the $^1H^C$ magnetization transfer pathway of eq 4.

Full relaxation matrix analysis[32,33] coupled with the kinetic exchange of the labile protons with water was performed by the numerical integration of eq 2. The calculated recovery of the $^1H^N$ magnetization indicates that the significantly shorter optimal interscan d_1 delays are achieved in the longitudinal relaxation optimized experiments as it is compared to the

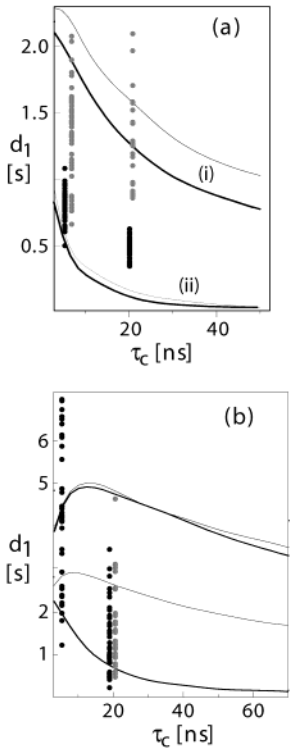

Figure 4. Optimal interscan ^{1}H relaxation delays, d_1, versus the protein rotational correlation time of a model protein (ubiquitin, PDB code 1UBI) calculated using the full ^{1}H relaxation matrix approach[32,33] coupled with the kinetic exchange of the labile protons with water (eq 2) (see the Methods section). The thin and thick lines represent two sets of calculations with the initial water magnetization fully saturated ($I_z^W(0) = 0$) or in the thermal equilibrium with the lattice ($I_z^W(0) = I_z^W{}_{eq}$), respectively. In (a), calculations are performed for the u-[^{15}N,^{13}C] labeled ubiquitin for two sets of initial conditions, (i), the initial magnetization of all ^{1}H spins is zero, (ii), the initial magnetization of $^1H^N$ spins is set to zero (upper curves) and the $^1H^C$ spins are in the thermal equilibrium with the lattice (lower curves). The curves represent the averaged recovery of all $^1H^N$ spins of ubiquitin. For calculations, the Lipari and Szabo spectral density function with $S^2 = 0.8$ and $\tau_e = 100$ ps are assumed. The experimentally determined optimal interscan ^{1}H relaxation delays for each individual $^1H^N$ spins of u-[^{15}N,^{13}C] labeled ubiquitin and u-[^{15}N,^{13}C] labeled BsCM are shown with gray and filled circles for the experiment of Figure 1b with and without ^{1}H saturation shortly after the $^1H^N$ acquisition. In (b), calculations are performed for the u-[^{2}H,^{15}N,^{13}C]-labeled ubiquitin in H_2O. The upper and lower curves correspond to the range of the calculated responses for each individual $^1H^N$ spin. The experimentally determined optimal interscan ^{1}H relaxation delays for each individual $^1H^N$ spins of u-[^{2}H,^{15}N,^{13}C]-labeled ubiquitin and u-[^{2}H,^{15}N,^{13}C] labeled BsCM are shown with gray and filled circles for the experiment of Figure 1b with and without ^{1}H saturation short after the $^1H^N$ acquisition.

standard experiments. In addition, a reduced dependence on the saturation level of water magnetization (thin and thick curves in Figure 4, parts a and b) is observed. A satisfactory correspondence between the measured optimal d_1 delays and the theoretical d_1 delays is obtained. Some deviation of the optimal interscan d_1 delays measured with ^{13}C,^{15}N-labeled and fractionally deuterated BsCM from the theoretical curve might originate from (i) the partial dilution of the $^1H^C$ spins by the ^{2}H spins, (ii) saturation of the $^1H^C$ spins of aromatic groups resonating close to the $^1H^N$ spins, and (iii) failure of the full relaxation matrix analysis to adequately represent spin dynamics in fractionally labeled proteins.[34] For the uniformly deuterated

(32) Olejniczak, E. T.; Gampe, R. T.; Fesik, S. W. *J. Magn. Reson.* **1986**, *67*, 28−38.
(33) Boelens, R.; Koning, T. M. G.; Kaptein, R. *J. Mol. Struct.* **1988**, *173*, 299−309.

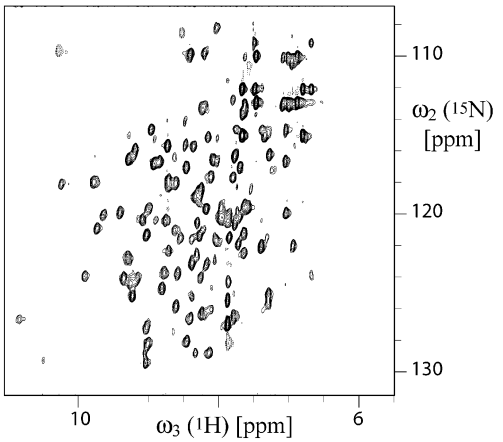

Figure 5. 2D [^{15}N,^{1}H]-projection of the 3D LTROSY−HNCA experiment of Figure 1c with the ^{1}H relaxation optimization applied to the u-[^{15}N,^{13}C]-labeled BsCM. The interscan ^{1}H relaxation delay $d_1 = 340$ ms. 12(t_1)*36-(t_2)*1024(t_3) complex points were accumulated yielding $t_{1max} = 5$ ms, $t_{2max} = 13$ ms and $t_{3max} = 51.2$ ms, respectively, and a total measurement time of 6 h (32 scans).

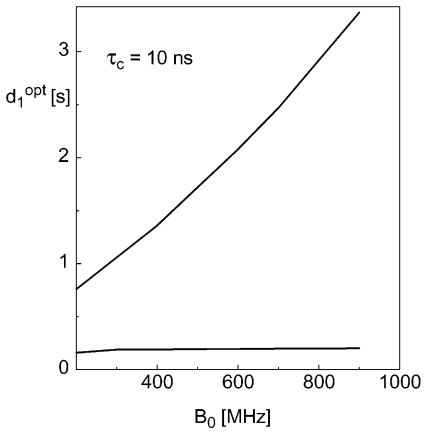

Figure 6. Optimal interscan $^{1}H^{N}$ relaxation delays, d_1, of a model protein (ubiquitin, PDB code 1UBI) versus polarizing magnetic field strength B_0 calculated using the full ^{1}H relaxation matrix approach (eq 2). The upper and lower curves correspond to the $^{1}H^{N}$ relaxation in LTROSY experiment of Figure 1a and conventional [^{15}N,^{1}H]-correlation techniques, respectively.

ubiquitin and BsCM, a wide distribution of the optimal interscan delays throughout the backbone $^{1}H^{N}$ spins is predicted and actually observed in the experiment (Figure 4b) resulting in a nonuniform appearance of the signal intensities in NMR spectra. Within the scope of the proposed approach this situation cannot be improved.

At high magnetic fields a viable solution to the longitudinal relaxation optimization can be obtained by the use of the $^{1}H^{N}$ band selective excitation pulses. Figure 5 shows 2D [^{15}N,^{1}H] projection of the 3D LTROSY−HNCA spectrum of ^{13}C,^{15}N labeled and 35% deuterated BsCM measured with the experimental scheme of Figure 1c. The uniform excitation via the $^{1}H^{N}$ region was obtained with the E-Burp2 and time reversed E-Burp2 pulses.[31] No active selection of the TROSY pathway was employed that would require implementation of additional $^{1}H^{N}$ selective 90° pulses. For the majority of the backbone amide groups of BsCM, the anti-TROSY cross-peaks were not detected due to strong transverse relaxation during the N−C magnetization transfer periods (Figure 5).

The source of enhanced longitudinal relaxation of $^{1}H^{N}$ spins to the steady-state level of the magnetization is the dipole−dipole interactions between the $^{1}H^{N}$ spins and all other ^{1}H spins in protein[8] and in bulk water.[18,35] The maximum effect is achieved when the magnetization of the $^{1}H^{N}$ group of spins is selectively perturbed from the corresponding thermal equilibrium. Frequently, this regime is called selective ^{1}H T_1 relaxation, which proceeds much faster and exhibits only small polarizing magnetic field strength dependence in contrast to nonselective ^{1}H T_1 relaxation, where the effects of dipole−dipole auto- and cross-relaxation tend to compensate each other.[36] Figure 6 compares the optimal interscan d_1 delays calculated as a function of the polarizing magnetic field strength B_o for the longitudinal relaxation optimized experiments and conventional experiments. Due to the increase of the nonselective longitudinal relaxation times of the ^{1}H spins in proteins with the magnetic field strength (Figure 6), the optimal interscan delays in the longitudinal relaxation optimized NMR experiments are of an order of magnitude shorter than that in the conventional experiments.

The concentration of the saturated protons is almost 5 times smaller than that of the protons with the corresponding magnetization returned back to the thermal equilibrium. Thus, in the spin-diffusion regime the dipole−dipole interactions between diluted $^{1}H^{N}$ spins and abundant "thermal bath" spins are not expected to perturb significantly the equilibrium state of the abundant spins. The effective longitudinal relaxation enhancement of the $^{1}H^{N}$ spins throughout entire multidimensional NMR experiments can be obtained provided that the magnetization of the thermal bath spins is maintained close to its thermal equilibrium or returned to the thermal equilibrium state before the signal acquisition as it is implemented in the experimental scheme of Figure 1, parts b and a, respectively. The dilution of the thermal bath ^{1}H spins with ^{2}H spins reduces the efficiency of the longitudinal relaxation optimization, so that the uniform deuteration of proteins should be undertaken with care. At 900 MHz, the predicted decrease of the $^{1}H^{N}$ longitudinal relaxation times can be as large as an order of magnitude making the proposed method a valuable tool for protein NMR at high magnetic fields.

Acknowledgment. Financial support was obtained from the ETH Zürich internal grant to K.P. We thank Silantes AG for providing us with the ^{15}N-, ^{13}C-, and ^{2}H(<35%)-labeled bacterial growth medium for the BsCM preparation. We thank Prof. Donald Hilvert and Alexander Kienhöfer, ETH Zürich, for the preparation of the NMR sample of BsCM.

Supporting Information Available: Figure illustrating that no improvement in S/N_t was observed in the case where all nonexchangeable protons were replaced with deuterons. This material is available free of charge via the Internet at http://pubs.acs.org.

JA027149Q

(34) Zolnai, Z.; Juranic, N.; Macura, S. *J. Biomol. NMR* **1998**, *12*, 333−337.
(35) Bruschweiler, R.; Wright, P. E. *Chem. Phys. Lett.* **1994**, *229*, 75−81.
(36) Rossi, C. Selective Relaxation Techniques in Biological NMR. In *Encyclopedia of Nuclear Magnetic Resonance*; Grant, D. M., Harris, R. K., Eds.; John Wiley & Sons: New York, 1996, p 4237−4246.
(37) Marion, D.; Ikura, M.; Tschudin, R.; Bax, A. *J. Magn. Reson.* **1989**, *85*, 393−399.
(38) Shaka, A. J.; Keeler, J.; Frenkiel, T.; Freeman, R. *J. Magn. Reson.* **1983**, *52*, 335−338.